



ELSEVIER

Physica D 165 (2002) 228–241

PHYSICA D

www.elsevier.com/locate/physd

The effect of cross-immunity and seasonal forcing in a multi-strain epidemic model

Masashi Kamo*, Akira Sasaki

Department of Biology, Graduate School of Science, Kyushu University, Fukuoka 812-8581, Japan

Received 26 July 2001; received in revised form 13 February 2002; accepted 18 February 2002

Communicated by Y. Kuramoto

Abstract

We study dynamical behavior and bifurcation structure of a multi-strain SIR epidemiological model with seasonal forcing in transmission rate. The conventional single strain SIR dynamics with seasonal forcing is known to show a cascade of bifurcations as the strength of seasonality increases. In this study with an extension to multiple strains of pathogens, we first investigate the bifurcation patterns of the two strain SIR model. In the two strain SIR model, a new parameter called cross-immunity between strains plays a key role in the dynamical behavior. As analogous to the single strain model, we found that the period doubling bifurcation occurs as the strength of seasonal forcing is increased. However, bifurcation patterns differ greatly both in their subharmonic periods and the relative phase of cycles between strains, depending mostly on the degree of the cross-immunity between strains. With strong and weak cross-immunities, the period doubling cascade proceeds gradually toward chaotic cycles. On the other hand, with intermediate cross-immunity, the loss of stability of annual cycle attractor is immediately followed by chaotic cycles. Asynchronous cycles of two strains are robust outcome when annual cycles lose stability, but the population can converge to perfectly synchronized biennial cycles if two strains are antigenically distant from each other. Second, we found that there are simultaneously stable multiple attractors in two strain SIR model. Biennial and chaotic attractors, e.g., occasionally coexist at the same degree of seasonal forcing, and the trajectories converge to one of them depending on the initial conditions. Such multiple attractors are widely seen between biennial and annual cycles, or among the different types of biennial cycles, at the same strength of the seasonality. Finally, we found that the population may switch from one attractor to another by introducing a small random noise in seasonally varying transmission rate. © 2002 Elsevier Science B.V. All rights reserved.

Keywords: Seasonal forcing; Multi-strain SIR model; Cross-immunity; Multiple attractors

1. Introduction

Echoviruses are known as a causative agent of the aseptic meningitis epidemics in Japan. Their outbreaks in Japan show seasonality: the reported number of infected hosts becomes the largest mostly in July (Fig. 1A). The seasonality in outbreak is common

among infectious disease, as in the widely known example of flu outbreaks.

Many epidemiological models have been studied to account for the sustained oscillation in the number of infected hosts (e.g. [1–5]). These models reveal that the introduction of seasonally varying transmission rate, e.g., well explain the annual, the biennial, and the other periodicity in the outbreaks of pathogen. Schwartz and Smith [3], e.g., showed in their SEIR model that the temporal pattern of the infected density is drastically changed by the strength of seasonality

* Corresponding author. Tel.: +81-92-642-2642; fax: +81-92-642-2645.

E-mail address: kamo@bio-math10.biology.kyushu-u.ac.jp (M. Kamo).

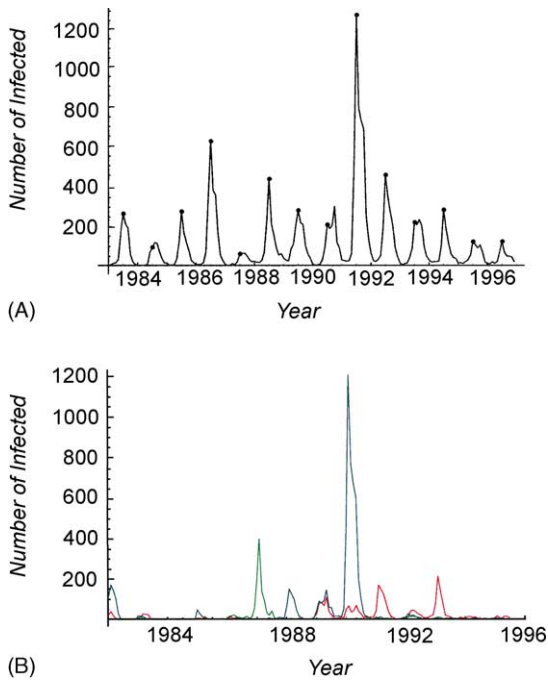


Fig. 1. (A) Monthly reported total number of people infected by echoviruses in Japan during the period 1982–1996. The black dots indicate the reported numbers in July. (B) Time changes in the morbidity of three echovirus sub-types, echo9 (green line), echo18 (red), and echo30 (blue). Dominant sub-types change between years.

(also see for SIR model in [4,6]). However, these models have been focused only on the dynamics of the single strain epidemics. In the case of echovirus epidemics, there are almost 30 serologically defined sub-types (echo1, echo2, etc.), and the major types change year by year. A recent nationwide outbreak occurred in 1991 in Japan with the major type echo30. In 1992, however, very few echo30 infections have been reported, and instead, echo9 caused most of the infections [7].

Fig. 1A shows the reported numbers of infections of echovirus sub-types from 1983 to 1996 in Japan. Although there are 33 sub-types in echoviruses, three sub-types are shown in Fig. 1B. A roughly ordered emergence by a set of sub-types is a characteristic of the echovirus outbreaks—the same sub-type tends to reemerge for about every 10 years. This contrasts with the pattern of outbreaks by influenza A viruses,

in which each year’s nationwide outbreak is caused by a new type which is slightly deviated from the last year’s major strain [8]. To understand the dynamics of those epidemics caused by a set of antigenically diverse sub-types, the extension of mathematical models is necessary.

Schwartz and Smith [3] showed that seasonal forcing causes the period doubling in the density of infected hosts by using the single strain SEIR model. In this study, we focus on an effect of the seasonal forcing in the single and multiple strain SIR model to investigate the pattern of the period doubling or the bifurcation in the host density. The reason why we used the SIR model rather than the SEIR model is that it is easier to extend to the multi-strain model which is not analyzed in [3].

When we consider the multiple strain model, we need a new parameter called cross-immunity between strains. Usually, once a host is infected by a certain viral strain, the host will be never infected by the same strain because of the acquired immunity for it. The immunity works to other viral strains which are antigenically close to the original one and hence the host will be rarely infected by such strains, although the immunity is less effective generally than to the original strain. This phenomenon is called cross-immunity.

In this study, we focus on the effect of seasonal forcing and the effect of the new parameter, cross-immunity. First, we investigate the conventional single strain SIR model and the way the bifurcation occurs by increasing the degree of the seasonality. Then the model is extended to a two strain model.

2. SIR model

We first introduce a conventional SIR model with seasonality. The densities of the susceptible (S), the infected (I) and the recovered (R) hosts change with time as

$$\begin{aligned} \dot{S} &= -\beta SI - \mu S + \mu, & \dot{I} &= \beta SI - \gamma I - \mu I, \\ \dot{R} &= \gamma I - \mu R, \end{aligned} \tag{1}$$

where \dot{x} represents the time derivative, β the transmission rate, μ the natural death rate and γ the recovery rate. The newborns are susceptible and the number of births and deaths are balanced. The total host density is scaled to 1. Throughout the paper we assume that the basic reproductive ratio, $R_0 = \beta/(\mu + \gamma)$, is greater than 1. Because echovirus shows strong seasonality in morbidity, we introduce the seasonal change in transmission rate:

$$\beta = \beta_0(1 + \delta \sin 2\pi t), \quad (2)$$

where β_0 is the base transmission rate, and $\delta(0 \leq \delta \leq 1)$ measures the degree of seasonality. The time is scaled in units of years, so the period of seasonal forcing is 1. It is well known that the SEIR model with the seasonality shows the diversity of dynamical behavior depending on the strength of the seasonality [3].

The annual cycle around the endemic equilibrium is stable when δ is sufficiently small. When δ exceeds a certain threshold, a 2-year cycle emerges. By further increasing δ , the system shows a cascade of period doubling bifurcation (2 years, 4 years, 8 years, etc.) towards chaos. We expect a similar bifurcation structure in the SIR model as the strength of the seasonality is increased. Fig. 2 illustrates the bifurcation diagram of the density of infected host when δ is varied, which we explain later in greater detail, in comparison with that of two strain model.

When this SIR model is extended to two strain model, the system is described by nine host compartments of different immunological status (SS, SI, SR, \dots, RR , where SI , e.g., represents the hosts which are susceptible to the strain 1 and infected by the strain 2). Introducing a new parameter σ that expresses the

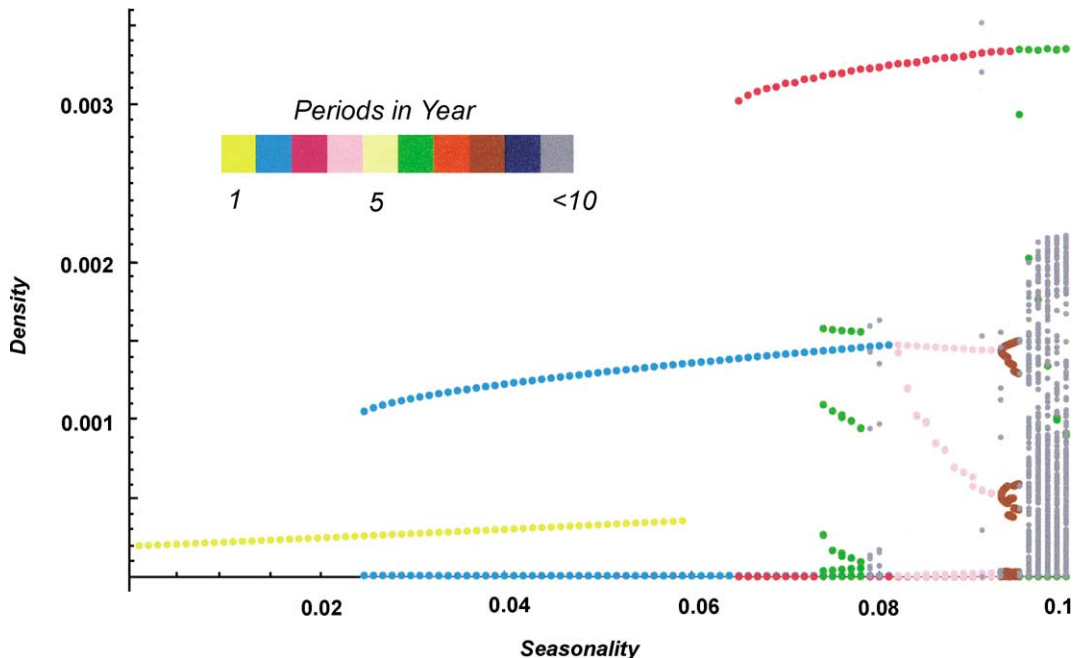


Fig. 2. The bifurcation diagram of single strain SIR model. Horizontal axis shows the strength of the seasonality and the vertical axis shows the densities of the infected hosts. The periods of years cycle are shown in a small color panel in the figure, and the numbers under the panel shows the period. More than 10 years cycles are shown in black dots. The parameters used in the simulation were $\beta = 1500$, $\gamma = 50$, $\mu = 0.01$. The time is measured in units of years, so the parameters correspond to an infectious disease with the mean infectious period $1/\gamma = 1$ week, the basic reproductive ratio $R_0 = \beta/(\mu + \gamma) = 30$ in the host with the mean life time $1/\mu = 100$ years. The parameters are nearly the same as in [3].

effect of cross-immunity, we have

$$\begin{aligned}
 \dot{x}_{SS} &= -\beta_1 x_{SS} x_{I\bullet} - \beta_2 x_{SS} x_{\bullet I} - \mu x_{SS} + \mu, \\
 \dot{x}_{IS} &= \beta_1 x_{SS} x_{I\bullet} - \beta_2 \sigma x_{IS} x_{\bullet I} - (\gamma_1 + \mu) x_{IS}, \\
 \dot{x}_{RS} &= \gamma_1 x_{IS} - \beta_2 \sigma x_{RS} x_{\bullet I} - \mu x_{RS}, \\
 \dot{x}_{SI} &= \beta_2 x_{SS} x_{\bullet I} - \beta_1 \sigma x_{SI} x_{I\bullet} - (\gamma_2 + \mu) x_{SI}, \\
 \dot{x}_{II} &= \beta_1 \sigma x_{SI} x_{I\bullet} + \beta_2 \sigma x_{IS} x_{\bullet I} - (\gamma_1 + \gamma_2 + \mu) x_{II}, \\
 \dot{x}_{RI} &= \beta_2 \sigma x_{RS} x_{\bullet I} + \gamma_1 x_{II} - (\gamma_2 + \mu) x_{RI}, \\
 \dot{x}_{SR} &= \gamma_2 x_{SI} - \beta_1 \sigma x_{SR} x_{I\bullet} - \mu x_{SR}, \\
 \dot{x}_{IR} &= \beta_1 \sigma x_{SR} x_{I\bullet} + \gamma_2 x_{II} - (\gamma_1 + \mu) x_{IR}, \\
 \dot{x}_{RR} &= \gamma_1 x_{IR} + \gamma_2 x_{RI} - \mu x_{RR}, \tag{3}
 \end{aligned}$$

where x_{SS} , e.g., is the density of hosts that are susceptible to both strains (SS). $x_{I\bullet} = x_{IS} + x_{II} + x_{IR}$ and $x_{\bullet I} = x_{SI} + x_{II} + x_{RI}$, respectively, are the total number of the strain-1-infected and the strain-2-infected hosts, and β_i and γ_i are the transmission rate and the recovery rate of the strain i ($i = 1, 2$). The new parameter σ (more precisely, $1 - \sigma$) stands for the degree of cross-immunity between strains 1 and 2. When $\sigma = 0$ (perfect cross-immunity), the hosts once infected by one strain will never be infected by the other strain. When $\sigma = 1$ (no cross-immunity), in contrast, two strains can independently infect the host. Again, the seasonality is introduced as in Eq. (2): $\beta_i = \beta_i^0 (1 + \delta \sin 2\pi t)$. If the cross-immunity is very strong ($\sigma \approx 0$), the competition between two strains becomes very strict. The strain with a smaller basic reproductive ratio would then go extinct [9,10]. However, as imperfect cross-immunity ($\sigma > 0$) strongly promotes the coexistence of strains, quite a large difference in the basic reproductive ratios is necessary in order that one of the strains go to extinction [10]. This competitive exclusion under an extremely strong cross-immunity condition is not the major interest of this study (because then two strains are antigenically indistinguishable). We therefore later assume symmetric parameters between two strains (by which the basic reproductive ratios of both strains are the same, and two strains always coexist except when σ is strictly zero).

Before proceeding to the analysis, we note that the eight-dimensional system (3) can be reduced, without loss of any information, to a five-dimensional sys-

tem by introducing the following state variables: $x = x_{SS}$, the density of universally susceptible hosts; $y_1 = x_{IS} + x_{II} + x_{IR} \equiv x_{I\bullet}$ and $y_2 = x_{SI} + x_{II} + x_{RI} \equiv x_{\bullet I}$, the density of hosts infected by the strain 1 and strain 2, respectively; $z_1 = x_{IS} + x_{RS}$ and $x_2 = x_{SI} + x_{SR}$, the density of host exposed to the strain 1 but susceptible to the strain 2, and vice versa, respectively [11,12].

The system (3) is then rewritten as

$$\begin{aligned}
 \dot{x} &= (-\beta_1 y_1 + \beta_2 y_2)x + \mu(1 - x), \\
 \dot{y}_1 &= \beta_1(x + \sigma z_2)y_1 - (\mu + \gamma_1)y_1, \\
 \dot{y}_2 &= \beta_2(x + \sigma z_1)y_2 - (\mu + \gamma_2)y_2, \\
 \dot{z}_1 &= \beta_1 x y_1 - \beta_2 \sigma z_1 y_2 - \mu z_2, \\
 \dot{z}_2 &= \beta_2 x y_2 - \beta_1 \sigma z_2 y_1 - \mu z_1. \tag{4}
 \end{aligned}$$

The following analysis is based on these equations (4), rather than (3).

3. Results

3.1. Phase diagram

We first study the single strain SIR model using Eq. (2). The way of bifurcation in the corresponding SEIR model have been well studied by Schwartz and Smith [3]. We reproduced similar results in our SIR model when strength of the seasonality is varied.

Starting with randomly assigned host densities of each state ($=S, I, R$), we simulated the SIR model for a few hundred years until the system reached asymptotic orbit. Then we investigate the period and the amplitude for the fluctuation in the density of the infected hosts. Fig. 2 shows the bifurcation diagram, where the horizontal axis shows the strength of the seasonality and the vertical axis shows the maximum density in each year (around $t = n + 1/4$ ($n = 0, 1, 2, \dots$) or around July). Because we obtained the result by numerical simulations, only stable orbits are shown in the figure. Orbits of different periods are shown in different colors. We can see that multiple attractors can coexist for a given degree of seasonal forcing. For example, when seasonal forcing parameter (δ) is in the range $0.025 < \delta < 0.06$, 1-year cycle and 2-year

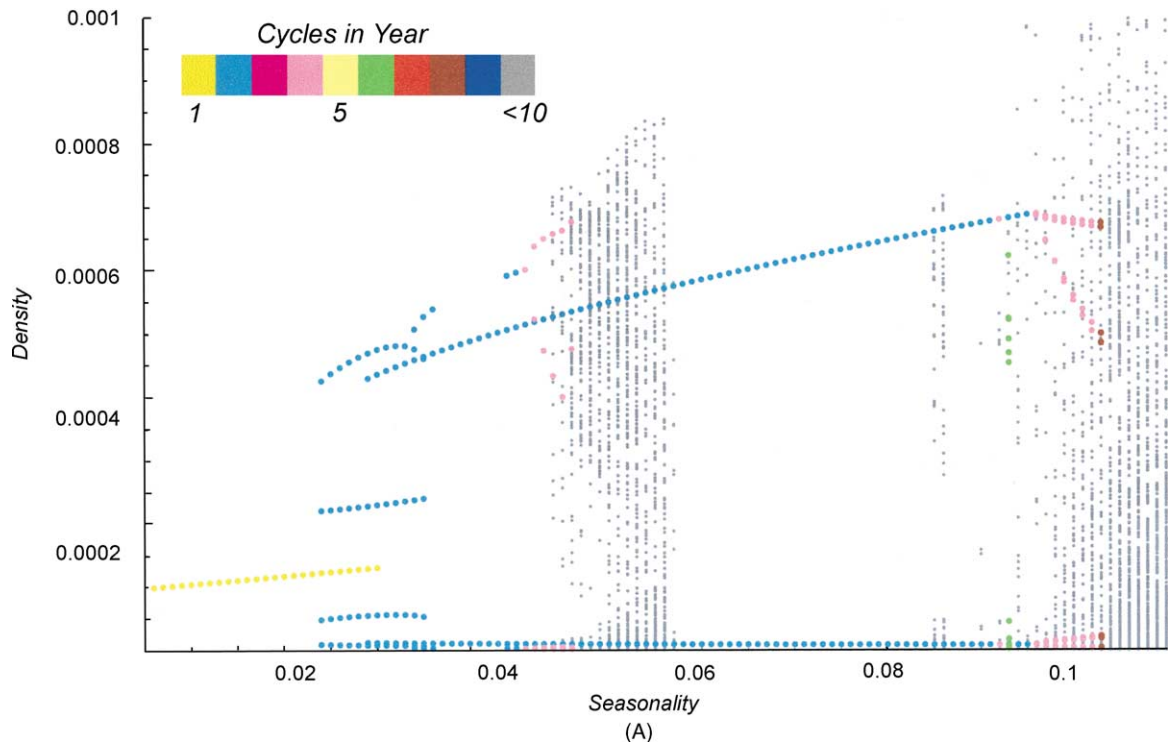


Fig. 3. The bifurcation diagram of two strains SIR model. We assumed symmetric parameters for both strain ($\beta_1 = \beta_2 = 1500$, $\gamma_1 = \gamma_2 = 50$, $\mu = 0.01$). Periods more than 10 years are shown in black dots. The density of only the first strain is shown. Since we assume the symmetric parameters between the strains, the diagram of the second strain is identical to the diagram. In these figures, for a given seasonality, we simulated the two strain SIR model for 50 runs with random initial condition. (A) The diagram when the cross-immunity parameter σ is 0.8. (B) $\sigma = 0.5$. (C) $\sigma = 0.1$.

cycle coexist, and a trajectory converges to one of the attractors depending on the initial condition.

The bifurcation diagrams in the two strain model were investigated in the same manner. Fig. 3 illustrates the bifurcation diagrams of two strain model for increasing δ , which retain the same tendency that were observed in the one strain SIR model. The population shows the annual cycle when the seasonality is sufficiently small, shows 2-year, 4-year cycles, and the cycles of still longer periods for intermediate strength of seasonality, and shows chaotic behavior for sufficiently strong seasonality. However, the bifurcation diagram shifts more quickly to chaos in the two strain model than in the single strain model by increasing the degree of seasonality, and shows more complicated bifurcations than that in Fig. 2 for the single strain case. In Fig. 3, only the density of hosts infected by

the strain 1 is shown because we assumed symmetric parameters for both strains ($\beta_1 = \beta_2$, $\gamma_1 = \gamma_2$) and hence the strain 2 shows the identical diagram (note, however, that their phases can be different, as we will see later). In these figures, we observe multiple attractors (e.g. both the annual and the biennial cycles are stable, and the trajectory is attracted to one of them depending on the initial state).

Fig. 3 also illustrates how the strength of cross-immunity affects the dynamical behavior (the panels in Fig. 3 only differ in their strength of cross-immunity). Again, starting with randomly assigned host densities, we simulated the two strain SIR model until a trajectory reaches a stable orbit. We replicated 50 independent runs with different initial conditions for a given seasonal forcing parameter and investigated period and amplitudes.

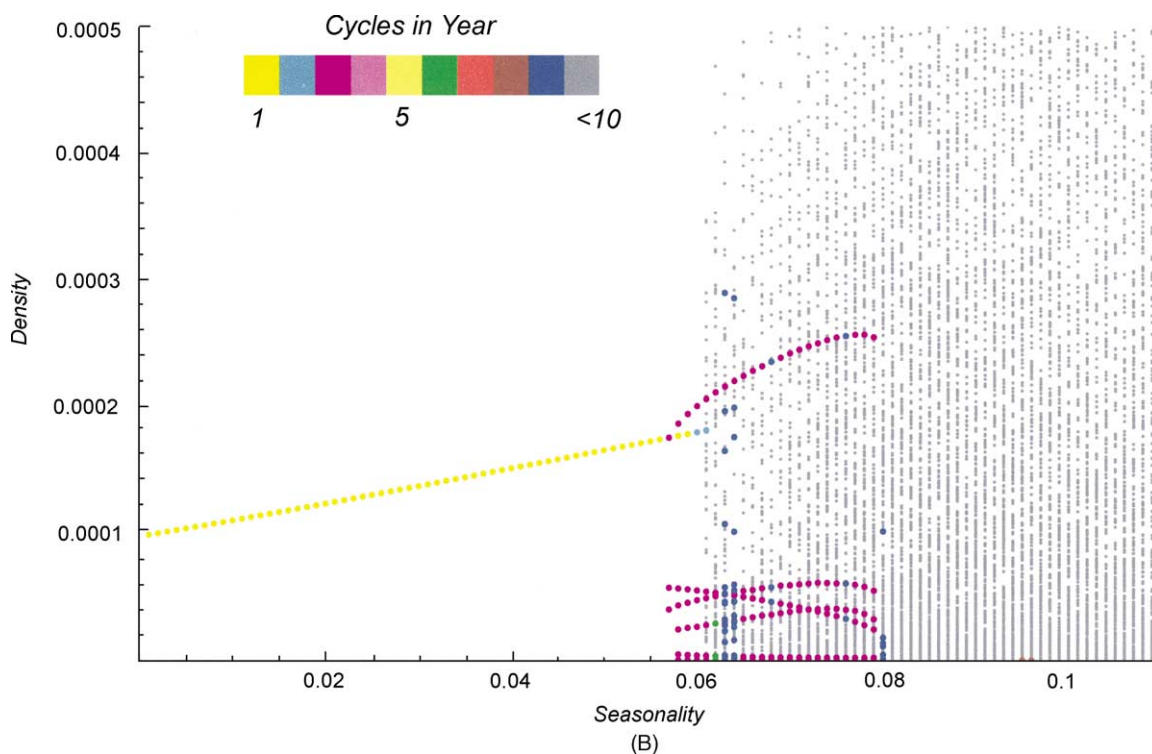


Fig. 3. (Continued).

If the cross-immunity is very weak ($\sigma \approx 1$), two strains behave almost independently with each other because each strain can freely infect the host that has been infected by the other strain. In contrast, if the cross-immunity is nearly perfect ($\sigma \approx 0$), two strains are antigenically indistinguishable, and hence when the infected densities are pooled together, the dynamics becomes almost identical to the single strain model, though the density is halved from the single strain model. With a weak cross-immunity shown in Fig. 3A, the chaotic behavior appears at a smaller seasonality parameter than in Fig. 3B for a medium cross-immunity case. Both in weak (Fig. 3A) and a strong (Fig. 3C) cross-immunity cases, we observe a broad region of parameter for limit cycle attractors of short periods (mainly 2 years and 4 years), although the 2-year cycles are not seen in Fig. 3C. On the other hand, with an intermediate strength of the cross-immunity (Fig. 3B), we observe a wide region of parameter

for 1 year, which suddenly bifurcates to the chaotic attractor.

3.2. Multiple attractors

In the two strain SIR model, when the trajectory is attracted to a limit cycle with more than 2-year period, we found that two strains may fluctuate with different phases. Trivially, if the dynamics shows 1-year cycle, two strains must fluctuate perfectly in-phase. When the dynamics shows a 2-year cycle, there are three kinds of attractors. In the first biennial cycle attractor, two strains fluctuate perfectly in-phase. In the second, two strains fluctuate in the opposite phases. In the third, two strains fluctuate asynchronously with completely different shapes. All these three 2-year cycle attractors coexist around $0.02 < \delta < 0.04$ —the trajectories converge to one of them depending on the initial conditions (Fig. 3A). One of the attractors disappears around $\delta = 0.03$ but appears again around $\delta = 0.035$.

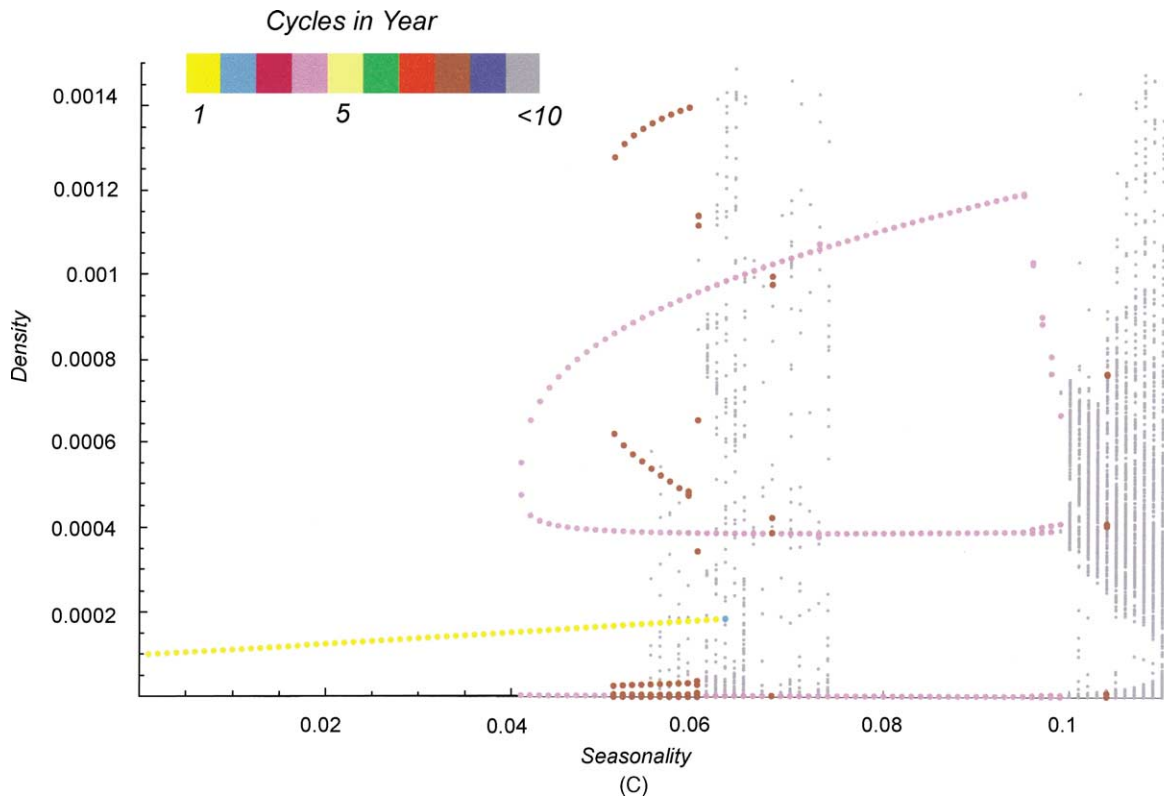


Fig. 3. (Continued).

The detailed bifurcation diagram is illustrated in Fig. 4A. The following procedure is used for the ‘continuation’ of the branches along the seasonality parameter in Fig. 4A. After the trajectory reaches a stable attractor for a certain seasonality parameter, we sampled the densities at the last time point, which are then used as the initial conditions for slightly different seasonality parameters. Because the changes in the seasonality parameter between simulations are very small, we expect that the trajectory converges to the same attractor. This process is repeated until an attractor of the 2-year period becomes unstable, or disappears.

3.2.1. Three kinds of biennial cycles

Three different kinds of branches for the biennial cycles are shown in Fig. 4A. A branch labeled as ‘S’ shows an attractor where the dynamics of two strains fluctuate perfectly in-phase with 2-year period. The

branch has a characteristic of the period doubling to 4 years cycles. When we further increase the seasonal forcing, the family of this branch finally bifurcates to a chaotic trajectory around $\delta = 0.05$ (see Fig. 3A). This chaotic attractor disappears around $\delta = 0.06$. A branch labeled as ‘A’ is an attractor in which the two strains fluctuate in opposite phase. This anti-phase 2 years cycle attractor lasts longer than the other 2-year cycles. The last branches labeled with ‘D’ show an attractor in which the two strains have different shapes of fluctuations, hence two branches are drawn in the diagram. An example of such trajectories is shown in Fig. 4B.

3.2.2. Biennial and chaotic attractor

The biennial cycles and chaotic attractor coexist around $0.05 < \delta < 0.06$ (Fig. 3A). We simulated the SIR model for 100 runs with randomly varied initial conditions at $\delta = 0.055$ and $\sigma = 0.8$, leading to 58

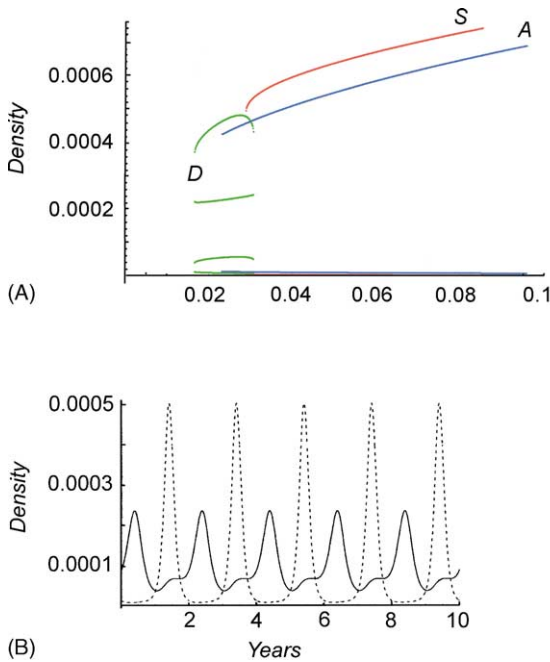


Fig. 4. (A) The branches of period of 2 years. The cross-immunity parameter: $\sigma = 0.8$. Horizontal axis shows the strength of seasonality (δ) and vertical axis shows the density of hosts infected by strain 1 in July ($t = n + 1/4, n = 0, 1, \dots$). The branch with ‘A’, shows the density in which two strains fluctuate in opposite phases. The branch with ‘S’, that with perfectly in-phase. The branches with ‘D’, two strains fluctuate in different wave shapes. The panel B shows trajectories of two strains in the branch ‘D’.

runs converging to biennial cycles and the others to the chaotic attractor.

When the dynamics is attracted to cycles with a period longer than 3 years, we do not observe any trajectories in which the two strains fluctuate in-phase. The phase relation between two strains would be expected as to have some systematic contribution to the bifurcation structure; however, we have not analyzed it yet.

3.3. Natural frequency and the resonance

3.3.1. Eigenvalues of the linearized system

When there is no seasonal forcing, the dynamics converges to a fixed point with a damped oscillation. The sustained oscillation of large amplitude is brought into the system by the seasonally varying transmission

rate that amplifies the natural frequency component of the system. In Fig. 5A, we plot the natural frequencies of the unforced system (the imaginary parts of the complex conjugate eigenvalues of the Jacobian for the dynamics (4) at the fixed point) as a function of cross-immunity parameter σ (shown in vertical axis). The fixed point of Eq. (4) with symmetric parameters, $\beta_1 = \beta_2, \gamma_1 = \gamma_2$, is

$$\begin{aligned} \hat{x} &= \frac{2 - \sigma - 2\sigma R + Q}{4(1 - \sigma)R}, \\ \hat{y}_1 = \hat{y}_2 &= \left(\frac{\mu}{\mu + \gamma} \right) \frac{-2 - \sigma + 2\sigma R + Q}{4\sigma R}, \\ \hat{z}_1 = \hat{z}_2 &= \frac{2 - 3\sigma + 2\sigma R - Q}{4R\sigma(1 - \sigma)} \end{aligned} \quad (5)$$

with $Q = \sqrt{4 - 4\sigma + (1 - 2R)^2\sigma^2}$ and $R = \beta/(\mu + \gamma)$.

Among five eigenvalues of the Jacobian around the fixed point (5) of this two strain SIR model, two pairs are conjugate complex numbers. We then expect that the natural frequencies associated with these two pairs of conjugate complex eigenvalues would be amplified when forced by seasonality. We denote these eigenvalues by

$$\begin{aligned} \lambda_{\pm}^{(1)}(\sigma) &= \nu_1(\sigma) \pm i\omega_1(\sigma), \\ \lambda_{\pm}^{(2)}(\sigma) &= \nu_2(\sigma) \pm i\omega_2(\sigma), \end{aligned} \quad (6)$$

where both ν_1 and ν_2 are negative for all σ , and ω_1 and ω_2 the natural frequencies of the linearized system. As we will see in the next section, ω_1 corresponds to the natural frequency of synchronized fluctuation of two strains, and ω_2 corresponds to the natural frequency for the anti-phase fluctuation of two strains. As shown in Fig. 5A, the first natural frequency ω_1 does not sensitively depend on the cross-immunity parameter σ , but the second natural frequency ω_2 does. Indeed, the approximation for small host death rate compared to the infection rates and the recovery rates, and large enough basic reproductive ratio (i.e. $\mu \ll \gamma \ll \beta$ —as expected in many human infectious diseases, see also [13,14]) reveals the following leading term for

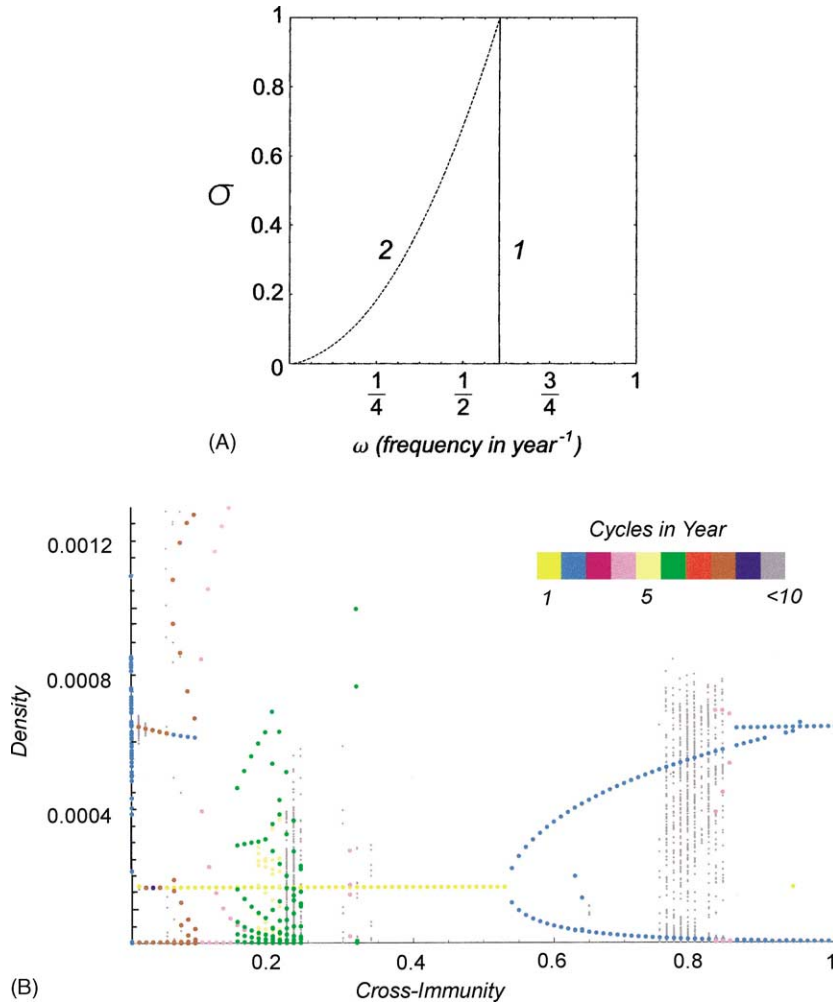


Fig. 5. (A) The σ dependence of the imaginary parts of the eigenvalues (natural frequencies) of Jacobian matrix of Eq. (4). The characteristic periods ($2\pi/\omega_i$) rather than frequencies are plotted in the horizontal axis in unit of years, as functions of cross-immunity parameter σ (vertical axis). There are two pairs of conjugate complex eigenvalues with the imaginary parts ω_1 and ω_2 , respectively. ω_1 is insensitive to the degree of cross-immunity σ and ω_2 sensitively depends on it— ω_2 is a monotonically increasing function of σ . Two natural frequencies coincide as σ approaches 1. (B) Bifurcation diagram with the cross-immunity parameter σ as the horizontal axis. Parameters are the same as in Fig. 3, except that the strength δ of the seasonality being fixed at 0.05. For the range of σ in which the second natural frequency (for asynchronous oscillation mode of two strains), ω_2 in (A), is close to 1/8 (cycle per year), the asynchronous cycles of period 8 are the major branch. For σ which gives rise to ω_2 close to 1/2, 2-year period cycles become the major attractors.

the friction coefficients and the natural frequencies:

$$\begin{aligned} \nu_1 &\approx -\frac{(2-\sigma)\mu\beta}{2\gamma}, & \omega_1 &\approx \sqrt{\beta\mu}, \\ \nu_2 &\approx -\frac{\sigma\mu\beta}{2\gamma}, & \omega_2 &\approx \sqrt{\beta\sigma\mu}. \end{aligned} \quad (7)$$

By inspecting the friction terms ν_1 and ν_2 , we see that the smaller σ is, the more pronounced is the con-

tribution of anti-phase oscillation mode with natural frequency ω_2 when the system is perturbed by an external periodical forcing, since the contribution of the i th natural frequency mode to the amplitude response of linearized system is

$$\frac{\nu_i}{\nu_i^2 + (\omega_i - \Omega)^2}, \quad (8)$$

where Ω is the angular frequency of the external forcing. In contrast the synchronized oscillation mode with natural frequency ω_1 becomes equally important as the anti-phase oscillation mode when σ approaches to 1.

Fig. 5B illustrates a bifurcation diagram for varying σ , when the seasonal forcing parameter, δ , is fixed at 0.05. When σ is small ($0 < \sigma < 0.01$), where the second natural frequency ω_2 is approximately 1/8 cycle per year, we found that the asynchronous limit cycles of period 8 are indeed one of the major branches in the bifurcation diagram obtained from the simulations. When σ becomes larger ($\sigma > 0.5$), both synchronous and asynchronous 2-year cycles constitute the major branches, as expected from Eq. (7). Although the precise bifurcation pattern accords only roughly with Eq. (7) and Fig. 5A, the figure clearly demonstrates the importance of the second natural frequency (and the friction coefficient) in determining the phases and periods of multi-strain epidemiological outbreaks.

A linear system with a sinusoidal external force should never show any subharmonic response. However, a trajectory of the forced nonlinear system (4) should have various subharmonic components (even in an annual cycle attractor, through non-sinusoidal shape of oscillation), which then “forces” the system itself having the resonance structure described above. The above analysis gives us key information for understanding which subharmonic mode and which phase relationship between the strains tend to predominate in the attractor, and how they change when the cross-immunity parameter σ is changed (see below).

3.3.2. Eigenvectors

Next we investigate the eigenvectors corresponding to these two kinds of complex eigenvalues. The corresponding eigenvectors are also complex. These complex eigenvectors give us information about both the phase and the amplitudes of fluctuation of the corresponding canonical mode. The elements of complex eigenvector \mathbf{u} corresponding to a pair of complex eigenvectors λ_{\pm} can be written as

$$\mathbf{u} = (|u_1|e^{i\phi_1}, |u_2|e^{i\phi_2}, \dots, |u_5|e^{i\phi_5})^T. \quad (9)$$

The second and the third elements of an eigenvector (9) correspond to the complex amplitude of y_1 and

y_2 , from which we can see the phases ϕ_2 and ϕ_3 of two strains in this canonical oscillation mode. We see from this that in the canonical oscillation mode corresponding to $\lambda_{\pm}^{(1)}$, two strains are perfectly in-phase (Fig. 6A), and in that corresponding to $\lambda_{\pm}^{(2)}$, two strains are perfectly out-of phase (Fig. 6B).

3.3.3. Natural frequencies and bifurcation structure

We here discuss how the natural frequencies of the linearized system for two strain SIR model (4) are related to the bifurcation structures observed in the numerical simulations. The analyses in the preceding sections are summarized as follows: (i) There are two pairs of conjugate complex eigenvalues, $\lambda_{\pm}^{(1)}$ and $\lambda_{\pm}^{(2)}$, of the linearized system. (ii) The natural frequency ω_1 of the first complex eigenvalue is insensitive to the changes in the degree of cross-immunity (σ), but the second natural frequency ω_2 depends critically on the cross-immunity. ω_2 is 0 when σ is 0, increases monotonically as σ increases, and finally approaches to the first natural frequency ω_1 as σ tends to 1 (also see Eq. (7)). (iii) The first natural frequency ω_1 corresponds to the canonical oscillation mode in which two strains fluctuate perfectly in-phase (Fig. 6A), and the second natural frequency ω_2 does to the canonical mode in which two strains fluctuate in perfectly opposite phases. (iv) The friction coefficient of anti-phase oscillation mode is small if σ is small, which increases monotonically with σ and approaches to the same value as the friction coefficient of synchronized oscillation mode as σ approaches 1. This indicates that the anti-phase subharmonic oscillation with a large period tends to be picked up in the attractor when σ is small (when cross-immunity is strong). For a large σ (weak cross-immunity), the anti-phase and the in-phase oscillation mode have comparable (and short) periods and the friction coefficients, suggesting that either two modes are mixed up in an attractor, or there exists bistability between the in-phase and the anti-phase oscillation attractors when σ is close to 1. To conclude, we expect that two antigenically distant strains can show synchronized outbreaks with a short period. By contrast, two antigenically close strains tend to keep the outbreak years away from each other, and the periods is likely to be longer. We will discuss later how

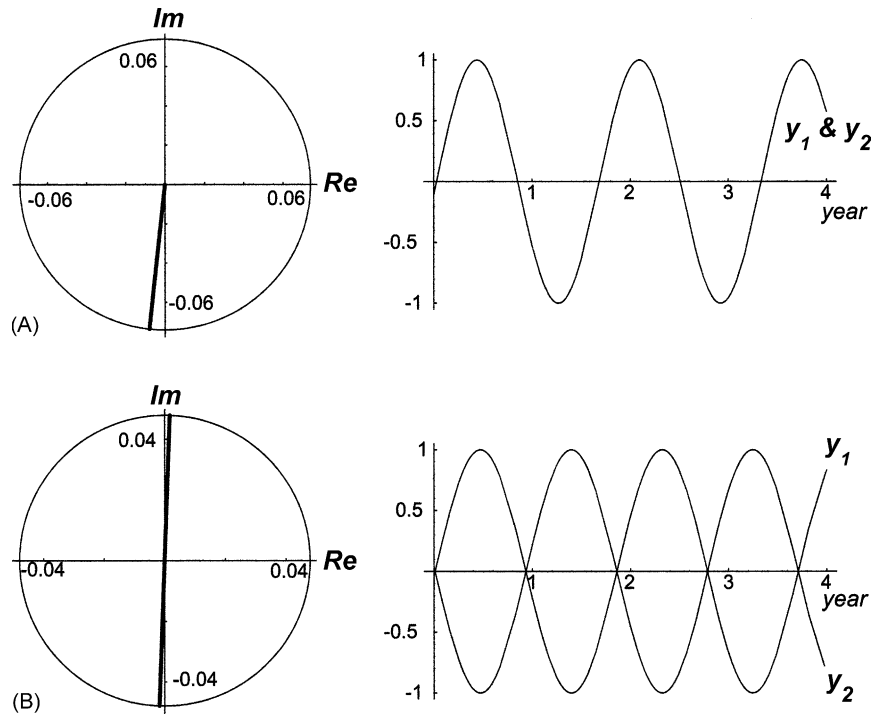


Fig. 6. Eigenvectors corresponding to the two natural frequencies ω_1 and ω_2 in Fig. 5A. This figure illustrates eigenvectors for $\sigma = 0.8$, but is qualitatively the same for all σ except $\sigma = 1$ and 0 . (A) The components of eigenvector for y_1 and y_2 , corresponding to ω_1 in Fig. 5A. In the left panel, axes show the real (horizontal) and imaginary parts (vertical) of eigenvectors. Two components coincide with each other, indicating that two strains fluctuate perfectly in-phase in this mode (right panel). The synchronized phases of strains 1 and 2 infected hosts are by about 90° lags behind that of universally susceptible hosts (SS). (B) The same as (A) but for the eigenvector corresponding to ω_2 . The fluctuations of both strains are perfectly in opposite phase (180°).

these predictions derived from the analysis of two natural frequencies agree with the bifurcation patterns of the dynamics (4) observed in numerical simulations.

3.4. Noise driven transitions between attractors

We here study the effect of small noise in seasonally varying transmission rate when there are multiple attractors. As is shown in Fig. 4A, even when the dynamics shows simple 2-year cycle, there are at least three different attractors for a given degree of seasonality. When we introduce noises in the transmission rate, we expect that a trajectory once converged to a certain attractor will be relocated to another attractor after being perturbed by noise, i.e. the transition between attractors may occur. Fig. 7 exemplifies such a transition between attractors indeed happens. The seasonal

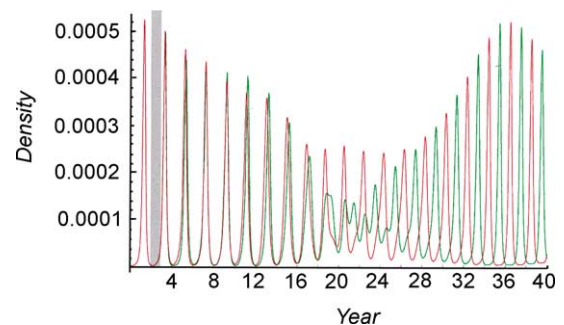


Fig. 7. An example of attractor transition. First, two strains fluctuate perfectly in-phase; then, the random noise is induced. By the noise, the transmission rate varies between -20 and $+20\%$ of its magnitude during the disturbance periods. The noise is introduced from the beginning to the end of the year 2 (shown in the gray box). After the noise introduction, the trajectory moves out of the in-phase attractor, and converges finally to the anti-phase biennial cycle attractor.

forcing parameter (δ) is 0.03 and the cross-immunity parameter (σ) is set to 0.8, at which in-phase biennial cycle is one of the stable orbits of the system (see Fig. 3A). The small noise is introduced to the infection rate from the beginning of the year 2 to the end of the year. Before they are exposed to the noise, the densities of two strains are in-phase, but after that they jumped to a different attractor in which they fluctuate in opposite phases. This kind of transitions between multiple attractors can also be seen between biennial and chaotic attractors as shown in Fig. 3. However, like the example in Fig. 7, the transition from in-phase to anti-phase is more likely to happen. As long as we investigate, the transition of the opposite way needs a larger amount of noise. We suspect that the basin of attraction for the anti-phase attractor would be larger than that of the in-phase attractor in this example.

4. Discussion

Forecasting the epidemics is a theoretically challenging issue particularly for the infectious diseases with great serotype diversity. There are at least 30 sub-types that caused the outbreaks of echoviruses during last two decades, and antigenically different mutants come up every year in the influenza outbreaks. Previous mathematical models for the population dynamics of infectious diseases, though highly successful in practice (e.g. [15,16]), have often focussed on a single strain dynamics—the multiple strain dynamics have often been ignored (but see [17] for the indirect interference between two different diseases).

For the practical purposes like the exploitation of the effective vaccination and the decision on the amount of vaccine stock in a year, the prediction on the morbidity and the major sub-type in the next year is critically important. A few studies have been directed to the forecasting of the epidemiological dynamics. Forecasting of single strain epidemiological dynamics is discussed in detail in [18,19], and the prediction of the major flu type in the next year from phylogenetic relationship (but not based on dynamics) is discussed by [8]. Only a few studies have focused on multiple strain epidemiological dynamics with cross-immunity

(e.g. [9–11,20]). The reason why the effect of multiple strain dynamics has been largely ignored in the literature is in its difficulty in coping with the enormous complexity of the dynamics, but without the effort of understanding the multiple strain dynamics, the prediction is of no use in many infectious diseases.

The seasonality is clearly important in echovirus epidemics (see Fig. 1). Theoretical studies on the epidemiological dynamics have revealed that the introducing of even a small amount of seasonal forcing in the epidemiological parameter drastically changes the temporal pattern (the annual, the biennial, and the other subharmonics) of outbreaks (e.g. [2,21]). Schwartz and Smith [3] analyzed the bifurcation structure of the SEIR model with seasonally varying transmission rate. They found that the population shows a cascade of period doubling bifurcation by increasing the strength of seasonality. However, the bifurcation structure of the multi-strain SIR model with seasonality has not been studied yet.

When we extend the SIR model to a multi-strain model, we have to consider the effect of cross-immunity. Most theoretical models with multiple strains have assumed either perfect cross-immunity (once a host acquires the immunity to a certain strain, it will never be infected by any other strains) or no cross-immunity (epidemiological processes of the strains are mutually independent). However, because sub-types are antigenically different (by definition), a host infected by a sub-type may be reinfected by another. The secondary infection rate becomes weaker than the primary one, the extent of which is determined by the degree of cross-immunity, i.e. by the serological distance between sub-types. The behavior of the multi-strain epidemiological dynamics critically depends on the coefficients of cross-immunity defined for each pair of sub-types (Fig. 3, also see [11,20]).

As we have mentioned before, there are two pairs of conjugate complex eigenvalues (and hence two natural frequencies, ω_1 and ω_2) in the two strain SIR model. The first natural frequency is insensitive to the changes in the degree of cross-immunity, but the second one monotonically increases as the degree of the cross-immunity is increased. These two natural frequencies play the key role in determining the pattern

of fluctuations of two strains (i.e. their periods and the relative phases).

Recall that the first natural frequency corresponds to the synchronized oscillation of two strains, and the second one corresponds to their anti-phase oscillation. We now compare the parameter dependences of ω_2 and the patterns of bifurcation observed in numerical simulations (Figs. 3 and 4). When σ is close to 0, ω_2 is small, so if this natural frequency is amplified by the seasonal (annual) fluctuation of transmission rate, we expect an outbreak of a long period (with perfectly opposite phases for two strains). For example, when $\sigma \approx 0.1$, the second natural frequency $\omega_2/2\pi$ (measured in cycles) is about 0.25 (= 1/4 cycle per year), hence the 4-year cycle with opposite phases for two strains is expected if the mode with ω_2 is to be amplified. This indeed accords with the first subharmonic branch in the cascade of bifurcations observed in the bifurcation diagram (see Fig. 3C). When the natural frequency $\omega_2/2\pi$ is about 0.5 (= 1/2 cycle per year) for $\sigma \approx 0.8$ (Fig. 5A), the anti-phase biennial cycle is one of the major branches in the bifurcation diagram (Fig. 3A, also see Fig. 4A). Seemingly, the fact that the second natural frequency ω_2 is close to ω_1 when σ approaches 1 would be responsible for the stimulation of the in-phase oscillation mode that corresponds to ω_1 , which is not excited for other region of σ . Thus when σ is close to 1, both the in-phase biennial cycles and the anti-phase biennial cycles are simultaneously stable, as well as their ‘interaction mode’ (different shape attractor (D) depicted in Fig. 4A).

Our conjecture from these observations is that there is a clear relationship between the natural frequencies, ω_1 and ω_2 , of the system and the observed bifurcation structure. We have not obtained mathematical justification so far for this claim, though we expect that it would be shown by a rigorous perturbation analysis of the system by making use of the averaging method.

Lastly, we would like to go back to our main purpose. Our aim is to forecast the dynamics of multi-strain epidemics like echoviruses (see Fig. 1). From the results of two strain model obtained in this paper, we may expect that the most antigenically dis-

tant strain from the currently abundant one tends to predominate in the next year or some later period in the same year, and antigenically close strains tend to have peak years away from each other. We, however, need to analyze the model with more than two strains to draw any conclusion for the order of outbreaks expected under a given antigenic distance relationship between strains. The most intriguing result, when the single strain SIR model is extended to multiple strain, is that there are multiple attractors in almost every parameter region we examined. Although, multiple attractors can be seen in the single strain model (see Fig. 2, such as between period of 1 and 2 years), the multi-strain case is more complicated. Even the attractors of simple 2-year period cycles and the chaotic one are occasionally coexisted in the same parameter set, and the trajectories once converged to one of the attractors would jump to another through a subtle modulation of trajectories by a random noise inevitable in the real world. This kind of transition between attractors is by no means specific to the multiple SIR model, and is also seen in the spatially coupled single strain SEIR model [22]. Earn et al. [22] showed that an introduction pulse vaccination in two-patch SEIR model can make the anti-phase biennial cycle in two patches to be synchronized. Analogously, we have shown that the transitions between attractors can be easily triggered by a small random noise in our seasonally forced two strain model (see Fig. 7). This would indicate the forecasting of the epidemics of multiple strains in noisy real world would become extremely difficult when the system allows multiple attractors.

The dynamics of the measles and other epidemics has been widely studied from the perspective of detecting chaos from noisy world (e.g. [18,19,23,24]). The difficulty in forecasting time series is often discussed from the sensitive dependence in initial data, which is inherent to the chaotic system. We have shown that even when the estimated Lyapunov exponents are negative so that the system has only stable attractors, the trajectories can be highly unpredictable—the transitions between multiple attractors driven by a small noise would be another robust source of unpredictability in such models as the multiple strain SIR model.

Still another difficulty would arise from the sensitive parameter dependence in the bifurcation diagram (e.g. Fig. 3). A slight change in the fitted parameter would totally change the prediction.

Acknowledgements

We thank Drs. Hiromu Yoshida, Yoshihiro Haraguchi, Mike Boots, Yoh Iwasa and an anonymous referee for their helpful comments. We also thank Isao Kawaguchi, Akiko Iwanaga, Emi Shudo and Akiko Satake for discussion. MK is supported by the post-doctoral fellowship from the Japan Society for the Promotion of Science.

References

- [1] H.W. Hethcote, J.A. Yorke, *Gonorrhea Transmission Dynamics and Control*, Springer, New York, 1980.
- [2] R.M. Nisbet, W.S. Gurney, *Modelling Fluctuating Populations*, Wiley, New York, 1982.
- [3] I. Schwartz, H. Smith, Infinite subharmonics bifurcation in an SEIR epidemic model, *J. Math. Biol.* 18 (1983) 233–253.
- [4] J.L. Aron, I.B. Schwartz, Seasonality and period-doubling bifurcations in an epidemic model, *J. Theoret. Biol.* 110 (1984) 665–679.
- [5] I.B. Schwartz, Multiple stable recurrent outbreaks and predictability in seasonality forced nonlinear epidemics models, *J. Math. Biol.* 21 (1985) 347–361.
- [6] M.J. Keeling, P. Rohani, B.T. Grenfell, Seasonally forced disease dynamics explored as switching between attractors, *Physica D* 148 (2001) 317–335.
- [7] *Infectious Agents Surveillance Report*, *Jpn. J. Med. Sci. Biol. Suppl.* 37–50 (1984–1997).
- [8] W.M. Fitch, R.M. Bush, C.A. Bender, N.J. Cox, Long term trends in the evolution of H(3) HA1 human influenza type A, *Proc. Natl. Acad. Sci. USA* 94 (1997) 7712–7718.
- [9] S. Gupta, J. Swinton, R.M. Anderson, Theoretical studies of the effects of heterogeneity in the parasite population on the transmission dynamics of malaria, *Proc. R. Soc. London B* 256 (1994) 231–238.
- [10] I. Kawaguchi, A. Sasaki, M. Boots, Why are dengue virus serotypes so distantly related? Enhancement and limiting serotype similarity between strains, submitted for publication.
- [11] V. Andreasen, J. Lin, S.A. Levin, The dynamics of cocirculating influenza strains conferring partial cross-immunity, *J. Math. Biol.* 35 (1997) 825–842.
- [12] C. Castillo-Chavez, H. Hethcote, V. Andraessen, S.A. Levin, W. Liu, Epidemiological models with age structure, proportionate mixing, and cross-immunity, *J. Math. Biol.* 27 (1989) 233–258.
- [13] V. Andreasen, Multiple time scales in the dynamics of infectious diseases, in: C. Castillo-Chavez, S.A. Levin, C.A. Shoemaker (Eds.), *Mathematical Approaches to Problems in Resource management and Epidemiology*, Springer, Berlin, 1989.
- [14] V. Andreasen, Age-dependent host mortality in the dynamics of endemic infectious diseases, *Math. Biosci.* 114 (1993) 29–58.
- [15] R.M. Anderson, R.M. May, *Population biology of infectious diseases: Part I*, *Nature* 280 (1979) 361–367.
- [16] R.M. Anderson, R.M. May, *Infectious Diseases of Humans*, Oxford University Press, Oxford, 1992.
- [17] P. Rohani, D.J. Earn, B. Finkenstadt, B.T. Grenfell, Population dynamics interference among childhood diseases, *Proc. R. Soc. London B* 265 (1998) 2033–2041.
- [18] S. Ellner, P. Turchin, Chaos in a noisy world: new methods and evidence from time-series analysis, *Am. Nat.* 145 (1995) 343–375.
- [19] S.P. Ellner, B.A. Bailey, G.V. Bobashev, A.R. Gallant, B.T. Grenfell, D.W. Nychka, Noise and nonlinearity in measles epidemics: combining mechanistic and statistical approaches to population modeling, *Am. Nat.* 151 (1998) 425–440.
- [20] Y. Haraguchi, A. Sasaki, Evolutionary pattern of intra-host pathogen antigenic drift: effect of cross-reactivity in immune response, *Phil. Trans. R. Soc. London B* 352 (1997) 11–20.
- [21] J.A. Yorke, N. Nathanson, G. Pianigiani, J. Martin, Seasonality and the requirements for perpetuation and eradication of viruses in populations, *Am. J. Epidemiol.* 109 (1979) 103–123.
- [22] D.J.D. Earn, P. Rohani, B.T. Grenfell, Persistence, chaos and synchrony in ecology and epidemiology, *Proc. R. Soc. London B* 265 (1998) 7–10.
- [23] G. Sugihara, R.M. May, Nonlinear forecasting as a way of distinguishing chaos from measurement error in time series, *Nature* 344 (1990) 734–741.
- [24] B.F. Finkenstadt, B.T. Grenfell, Time series modelling of childhood diseases: a dynamical systems approach, *J. R. Statist. Soc. C* 49 (2000) 187–205.